processes

MDPI

Article

Supercritical Foaming and Impregnation of Polycaprolactone and Polycaprolactone-Hydroxyapatite Composites with Carvacrol

Alina Satpayeva [1,2], Adrián Rojas [3,4,*], Marcin Tyrka [5], Ewelina Ksepko [5], María José Galotto [3,4] and Irena Zizovic [5,*]

1 Faculty of Science, Aix-Marseille University, 13013 Marseille, France; alina.satpayeva@uva.es
2 High Pressure Processes Group, Department of Chemical Engineering and Environmental Technology, University of Valladolid, 47011 Valladolid, Spain
3 Packaging Innovation Center (LABEN), Department of Science and Food Technology, Faculty of Technology, University of Santiago of Chile (USACH), Santiago 9170201, Chile; maria.galotto@usach.cl
4 Center for the Development of Nanoscience and Nanotechnology (CEDENNA), Santiago 9170124, Chile
5 Faculty of Chemistry, Wroclaw University of Science and Technology, 50-370 Wroclaw, Poland; marcin.tyrka@pwr.edu.pl (M.T.); ewelina.ksepko@pwr.edu.pl (E.K.)
* Correspondence: adrian.rojass@usach.cl (A.R.); irena.zizovic@pwr.edu.pl (I.Z.)

Abstract: Polycaprolactone (PCL) and polycaprolactone-hydroxyapatite (PCL-HA) scaffolds were produced by foaming in supercritical carbon dioxide ($scCO_2$) at 20 MPa, as well as in one-step foaming and impregnation process using carvacrol as an antibacterial agent with proven activity against Gram-positive and Gram-negative bacteria. The experimental design was developed to study the influence of temperature (40 °C and 50 °C), HA content (10 and 20 wt.%), and depressurization rate (one and two-step decompression) on the foams' morphology, porosity, pore size distribution, and carvacrol impregnation yield. The characterization of the foams was carried out using scanning electron microscopy (SEM, SEM-FIB), Gay-Lussac density bottle measurements, and Fourier–transform infrared (FTIR) analyses. The obtained results demonstrate that processing PCL and PCL-HA scaffolds by means of $scCO_2$ foaming enables preparing foams with porosity in the range of 65.55–74.39% and 61.98–67.13%, at 40 °C and 50 °C, respectively. The presence of carvacrol led to a lower porosity. At 40 °C and one-step decompression at a slow rate, the porosity of impregnated scaffolds was higher than at 50 °C and two- step fast decompression. However, a narrower pore size distribution was obtained at the last processing conditions. PCL scaffolds with HA resulted in higher carvacrol impregnation yields than neat PCL foams. The highest carvacrol loading (10.57%) was observed in the scaffold with 10 wt.% HA obtained at 50 °C.

Keywords: supercritical CO_2; polycaprolactone; hydroxyapatite; scaffold; foaming; impregnation; carvacrol

Citation: Satpayeva, A.; Rojas, A.; Tyrka, M.; Ksepko, E.; Galotto, M.J.; Zizovic, I. Supercritical Foaming and Impregnation of Polycaprolactone and Polycaprolactone-Hydroxyapatite Composites with Carvacrol. *Processes* **2022**, *10*, 482. https://doi.org/10.3390/pr10030482

Academic Editor: Maria Angela A. Meireles

Received: 30 January 2022
Accepted: 22 February 2022
Published: 27 February 2022

1. Introduction

Bone fractures are a global public health issue. In the last three decades, the incidence, prevalence, and years lived with disability increased 33, 70, and 65.3%, respectively, being women and older people the groups with a particularly higher risk of fractures [1]. According to considerable research, actual clinical treatments for bone repair and regeneration, autologous and allogeneic transplantations using autografts and allografts, have significant shortcoming, limitations, and complications [2,3]. Particularly, autografts possess the essential components to achieve osteoinduction and osteoconduction, but the process involves harvesting bone from the patient's iliac crest, which leads to a second operation at the site of tissue harvest. Meanwhile, autologous bone transplants are very expensive procedures with surgical risks such as bleeding, inflammation and infection, and also may result in significant donor site injury, morbidity, deformity, scarring, and chronic pain. Moreover,

none of the abovementioned approaches possess all of the ideal characteristics such as reasonable cost, low patient morbidity, easy post-operation access to the intervention, as well the use of materials with high osteoinductive and angiogenic potentials, biological safety and long shelf life [4].

In the last decades, polymer scaffold technology for tissue engineering has arisen as an alternative for the accelerated recovery of damaged bone tissues [4]. In order to have the ideal porous scaffold, it is important to have an interconnected porous structure, sufficient mechanical strength, and good cell-scaffold interaction. The main structural parameters of porous scaffolds for bone regeneration include pore size, pore morphology, and degree of porosity. Conventional methods for synthesizing highly porous and interconnected polymer scaffolds include solvent casting-particle leaching, freeze-drying, particle leaching, thermally induced phase separation, compression molding, injection molding, foaming extrusion, and electrospinning [5,6]. Moreover, drawbacks of the conventional methods include the use of large amounts of organic solvents and high temperatures [7]. In the last years, supercritical fluid technology has emerged as a highly attractive alternative to the conventional methods used for polymer processing [8,9]. A pure component is considered a supercritical fluid (SCF) if its temperature and pressure are higher than the critical values (Figure 1). When the compound's critical temperature and pressure are exceeded, the fluid shows specific properties such as the diffusivity and viscosity of a gas and the densities and solvating properties of liquids [10]. In most of the main applications of supercritical fluids, carbon dioxide (CO_2) is the most used fluid because it is non-toxic, non-flammable, inexpensive, and is a byproduct in ethanol and ammonia plants production. Thus, supercritical CO_2 ($scCO_2$) is considered a green solvent. Moreover, CO_2 has a very accessible critical point (P > Pc = 7.38 MPa and T > Tc = 304.15 K), which allows to carry out polymer processing at near-ambient temperature avoiding the thermal degradation of organic compounds (drugs, antimicrobials, antioxidants, etc.) [11,12].

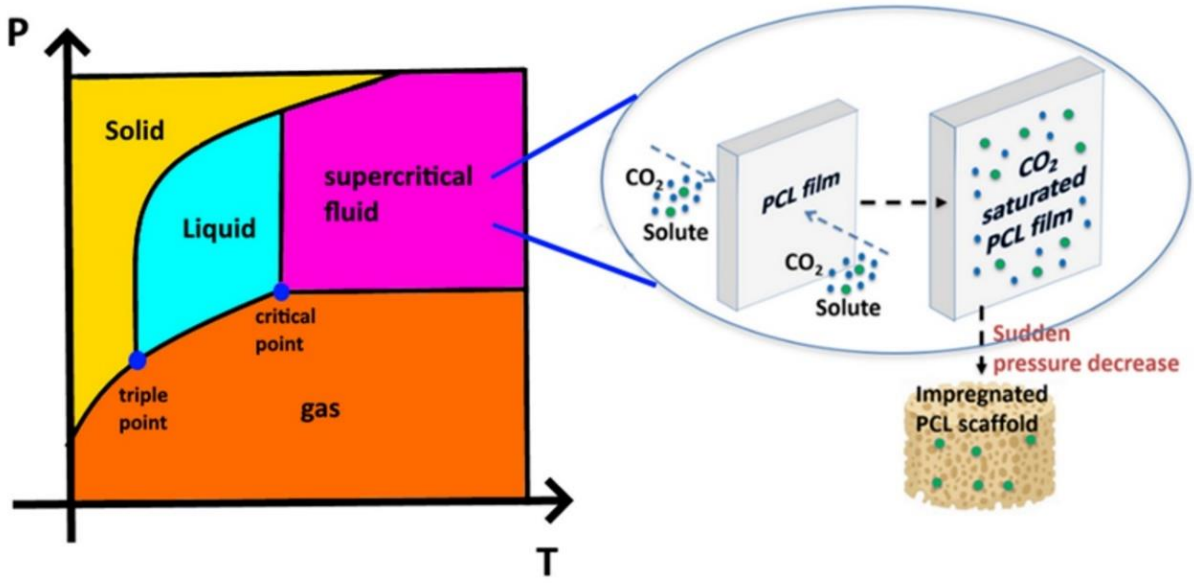

Figure 1. Pressure-temperature phase diagram and scheme of the simultaneous supercritical carbon dioxide ($scCO_2$)-assisted foaming and impregnation of polymers.

One of the most important applications of supercritical fluids corresponds to its use as a blowing agent for the production of scaffolds using thermoplastic polymers. Polymer foaming using $scCO_2$ can be carried out either at a lab-scale (batch foaming) for preliminary studies and at pilot-scale using supercritical continuous extrusion foaming [13]. Regardless of the foam processing method, the principles of the process are the same and can be explained in three stages. In the first stage, the polymer is saturated with $scCO_2$ (CO_2 absorption degree depends on the chemical affinity between polymer and

CO_2) and using foaming temperatures depending on the glass transition temperature for amorphous polymers and melting temperature for semicrystalline polymers. Then, in the second stage, a thermodynamic instability (a sudden increase of temperature or a rapid decrease of pressure) is introduced into the saturated polymer-scCO_2 mixture to induce cell nucleation due to the separation of phases caused by the reduction of CO_2 solubility (CO_2 supersaturation in the polymer). Finally, the third stage corresponds to the cell growth (depending on gas diffusion rate, viscoelastic behavior, etc.) and stabilization (depending on cell growth stresses and melt-strength) as gas diffuses from the polymer into the nucleated cells while the foam structure is gradually formed. Finally, the cell structure is stabilized by cooling [14].

Poly(α–hydroxy acids), such as poly (glycolic acid) (PGA), poly(lactic acid) (PLA the copolymer PLGA and poly (ε–caprolactone) (PCL) have been the most used polymers for the design of polymeric scaffolds for tissue regeneration by scCO_2-assisted foaming process because they are approved for clinical use by the US Food and Drug Administration (FDA) due to biocompatibility and degradation into non-toxic components [15]. Polycaprolactone is a semicrystalline aliphatic polyester with a low melting point of about 60 °C and a glass transition temperature (T_g) near to −60 °C, which make its processing easier [16,17]. PCL combined advantages for bone regeneration such as biocompatibility and the appropriate low bio-resorption rate that has favored its use to fabricate bone scaffolds. Nevertheless, PCL degrades significantly slower than PLA, PGA, and PLGA [18], which makes it less attractive for general tissue engineering applications but more attractive for long-term implants and controlled release applications. Therefore, to improve its functional properties for engineering tissue application, PCL must be blended with other materials. PCL-based copolymers have recently been synthesized to improve the degradation properties of PCL [19]. Also, nanotechnology has emerged as an alternative strategy to improve the functional properties of polymers used for tissue engineering applications. Particularly, bioactivity, osteo-conductivity, and bonding ability of PCL has been improved by the addition of hydroxyapatite (HA) nanostructures [7,17,20]. HA promotes bone ingrowth and is biocompatible because around 65 wt.% of bone is made of HA, $Ca_{10}(PO4)_6(OH)_2$ [21].

An additional challenge concerning the design of scaffolds for engineering tissue applications is the possibility of a bacterial infection in the surgical site, which has led to an increased interest in developing new scaffolds exhibiting antimicrobial activity [22,23]. The use of naturally occurring compounds with antibacterial activity has emerged as an alternative approach over synthetic antibiotics to control the spread of pathogenic organisms. Many natural compounds such as thymol, cinnamaldehyde, and carvacrol have been investigated for their antimicrobial activity. Carvacrol is a monoterpenoid phenol and the main component of the essential oil of oregano with a wide variety of biological properties, including anti-inflammatory, antioxidant, antitumor, antimutagenic, anti-parasitic, and antimicrobial activities [24–27]. It was reported to have significant antibacterial activity against both Gram-positive and Gram-negative bacteria, including methicillin-resistant staphylococci (MRSA) [28]. Additionallly, carvacrol has generally recognized as safe (GRAS) status by the Food and Drug Administration (FDA) [29]. Under normal conditions, carvacrol is a liquid with excellent solubility in scCO_2, which makes it an ideal candidate for the design of novel antimicrobial materials by the usage of scCO_2 [30].

Besides the possibility of polymer foaming, another advantage of scCO_2 is that it can be the most appropriate environment for impregnating polymers with active substances. The supercritical solvent impregnation (SSI) involves the dissolution of an active compound in a supercritical fluid and its contact with a polymer for its functionalization. Since no organic solvents are used in this process, high purity final products can be obtained [31–33]. SSI is a complex process that depends on the following parameters: pressure, temperature, rate of decompression, and interactions between the polymer and scCO_2 and between the polymer and the active component [12]. The polymer swelling due to exposure to scCO_2 allows the easy penetration of the dissolved active compound into the polymer matrix facilitated by the scCO_2-phase surface tension close to zero. Upon the decompression and CO_2 transfer

from a supercritical to a gas state, the solubility of the active component in CO_2 drops and it is trapped inside the polymeric matrix [34,35]. Besides this purely physical deposition mechanism, the molecular dispersion impregnation mechanism by hydrogen bonding or other electrostatic interactions between the active substance and the polymer could result in a high impregnation yield [36]. Described phenomena in $scCO_2$ utilization have motivated studies combining polymer foaming and impregnation in a one-step CO_2-assisted process (Figure 1) [35]. Ivanovic et al. reported that moderated pressures (13–17 MPa) and HA at 10 wt.% allowed obtaining well-dispersed microcellular composite PCL-HA scaffolds with mean pore sizes ranging between 200 and 300 μm. Thymol impregnation yields were in the range of 11 to 23.7 wt.%. Salerno et al. [37] reported that microstructural features of PCL scaffolds were highly affected by the HA content and temperature used. Particularly, highly porous PCL scaffolds with a narrow pore size distribution and adequate mechanical and biodegradability properties for bone tissue engineering applications were produced using temperatures higher than the melting point of the polymers. These authors reported PCL scaffolds with porosity values ranging from 55 to 85% and mean pore size from 40 to 250 μm using temperatures ranging between 37 and 40 °C and pressures between 10 and 20 MPa [38].

The biological properties of polymer scaffolds for tissue engineering applications depend on obtaining bimodal and highly interconnected foams. Pore sizes between 1 and 50 μm have been related with the promotion of nutrient and metabolic waste transfer in the interior parts of the pores, and pores with the size on the order of 100 μm have been associated with a significant impact on the in vitro cell invasion and differentiation [39–41]. In this context, a two-step depressurization foaming process has been proposed for the design of bi-modal and highly interconnected foams suitable as scaffolds for tissue engineering. In this process, the formation of large pores occurs during the first depressurization step's long foaming time; the second depressurization, which is very fast, causes the formation of small new pores and the further growth of the existing pores. PCL and PCL-HA nanocomposite scaffolds with bimodal and uniform pore size distributions were fabricated by quenching molten samples in liquid N_2, solubilizing $scCO_2$ in the molten samples at 37 °C and 20 MPa, and further releasing the blowing agent in two steps: (1) from 20 to 10 MPa at a slow depressurization rate, and (2) from 10 MPa to the ambient pressure at a fast depressurization rate [42]. Recently Garcia-Casas et al. [43] investigated $scCO_2$–assisted foaming and impregnation of PCL with quercetin. Quercetin release profiles showed that higher times were required to dissolve quercetin, demonstrating the efficacy of using a PCL scaffold to control the quercetin release kinetics. Campardelli et al. [44] reported that the release of nimesulide trapped into a PCL scaffold was delayed 3.5 times compared to the non-trapped drug. Controlled drug release profiles over several days were reported by Yoganathan et al. [45] from PCL samples impregnated with ibuprofen. The effect of operating conditions on the impregnation of ibuprofen into PCL was investigated over two pressure and two temperature levels, 150 and 200 bar, and 35 and 40 °C, respectively. Polycaprolactone with drug-loadings in the range from 2 to 27 wt.% were obtained.

In this framework, this study aimed to develop antibacterial PCL and PCL–HA composite scaffolds by their functionalization with carvacrol. The impregnated PCL scaffolds were obtained by a one-step $scCO_2$-assisted foaming and impregnation process using different temperatures, HA contents, and depressurization types. To our knowledge, this is the first study on the simultaneous supercritical foaming and impregnation of carvacrol in composite PCL scaffolds to be applied in tissue engineering applications.

2. Materials and Methods

2.1. Chemicals

PCL granules (M_n = 80,000) purchased from Sigma Aldrich (Steinheim, Germany) were used for the experiments. HA nanoparticles (Sigma Aldrich) with mean sizes lower than 200 nm were selected to prepare the PCL-HA composites. CO_2 (99.99% purity) was

used as blowing agents for gas foaming experiments. Carvacrol (purity ≥ 98%) was also supplied by Sigma-Aldrich. Acetone p.a. was purchased from (Stanlab, Lublin, Poland).

2.2. Preparation of PCL-HA Composites by Solvent Casting

Composite PCL-HA films were prepared by solvent casting using acetone. Briefly, PCL/acetone solution (1:10 *w*/*w*) was stirred at 1000 rpm for 1 h using a constant temperature (40 °C) to achieve a full polymer dissolution. Then, HA nanoparticles were added to the previous former PCL/acetone solution to obtain dry composite films with different HA contents (0, 10 and 20 wt.%) by solvent removal from a petri dish inside an oven working at 40 °C. A piece of wood was placed below the Petri dish as an insulator. While the oven provided a fast drying, the wooden insulation at the bottom yielded streams of evaporating acetone that lifted HA particles and prevented their deposition at the bottom of the dish. The obtained composite films were cut into small pieces for $scCO_2$ processing.

2.3. $scCO_2$-Assisted Foaming and Impregnation Assays

Figure 2 shows a scheme of the experimental setup used for the $scCO_2$-assisted foaming and impregnation assays. These processes were carried out in a 25 mL volume high-pressure view chamber (Eurotechnica GmbH, Bargteheide, Germany) with two sapphire windows. Around 0.4 g of layered square-shaped small pieces of PCL or PCL-HA films were put in a custom-made mold. In the case of simultaneous foaming and impregnation process, next to the mold with the polymer, approximately 0.8 g of carvacrol was put in another glass vessel. The process begins heating the high-pressure chamber using an electrical heating jacket rolled around the cell to guarantee a uniform temperature along with the high-pressure cell (40 or 50 °C). Then, CO_2 was pumped into the chamber from the gas cylinder through valve V1, and the system was pressurized using a driven gas booster until it reached 20 MPa.

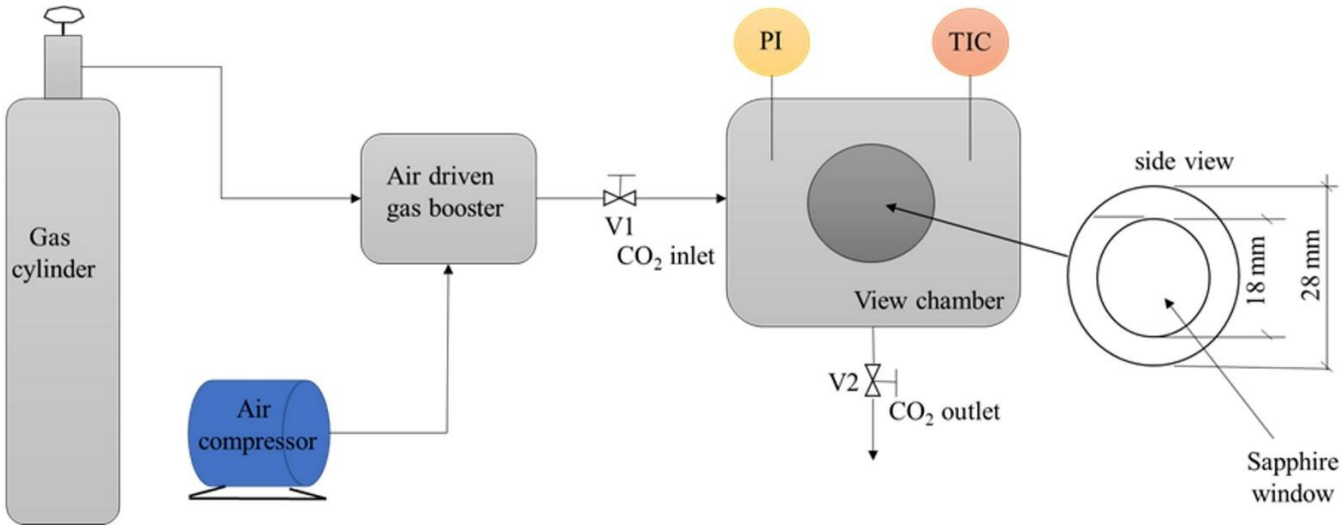

Figure 2. Scheme of the experimental setup used for one-step batch foaming and impregnation assays.

The system was kept at a constant temperature and pressure for a predetermined time: 1.5 h for foaming and 3 h for simultaneous foaming and impregnation. At the end of the process, valve V2 was opened manually to decompress the system to the atmospheric pressure. Two different modes of decompression were used: (1) one step slow decompression with the dP/dt = 0.5 MPa/min; (2) two steps decompression: from 20 MPa to 9 MPa with dP/dt = 0.5 MPa/min, and from 9 MPa to atmospheric pressure, dP/dt = 20 MPa/min. The process time and polymer and carvacrol quantities were defined in preliminary experiments (carvacrol was provided in excess). Experimental temperature and pressure were chosen based on our previous work on PCL impregnation [20,23]. The

experiments were performed in duplicates or triplicates. Experimetal parameters are summarized in Table A1 (Appendix A).

2.4. Foam Characterization

Pore morphology of the PCL and PCL-HA foams was investigated by scanning electron microscopy (Dual Beam SEM/Ga-FIB Microscope FEI Helios NanoLab™ 600i, FEI, FEI, Thermo Fisher Scientific, Eindhoven, The Netherlands). The microscope works under high vacuum conditions around 10^{-4} to 10^{-7} Pa. To investigate foams' cross-section, samples were cooled using CO_2 dry ice and cut by scalpel. Then, the samples were attached to an aluminum stage with copper tape and coated with a layer of gold with a thickness of 10 nm. Obtained SEM images were analyzed by a Java-based image processing program – ImageJ, which allowed to measure the pore size of the foams. The density of the scaffolds was determined by using a BLAUBRAND, Gay-Lussac density bottle (Sigma Aldrich). The following equation was used to calculate foam density (ρ_{foam}):

$$\rho_{foam} = \frac{\rho_{H_2O} \times w_1}{w_1 + w_2 - w_3} \quad (1)$$

where w_1 is the mass of the sample, w_2 is the mass of pycnometer and water, w_3 is the mass of glass with water and the sample. The density of water was also measured by pycnometer since its volume was known (V_{pyc} = 24.554 cm^3). Porosity was calculated using the following equation:

$$\varepsilon(\%) = \left(1 - \frac{\rho_{foam}}{\rho_{PCL}}\right) \times 100 \quad (2)$$

Impregnated mass of carvacrol was determined gravimetrically by measuring the impregnated sample. The impregnation yield (I) of PCL was calculated from Equation (3):

$$I(\%) = \frac{m_{carvacrol}}{m_{impregnated\ sample}} \times 100 \quad (3)$$

where $m_{carvacrol}$ is the mass of impregnated carvacrol calculated as the mass difference of the sample after and before the impregnation, and $m_{impregnated\ sample}$ is the mass of scaffold at the end of the process.

To confirm the presence of carvacrol on the surface of impregnated samples, FTIR and X-ray diffraction (XRD) analyses were performed. The IR spectra were recorded in the ATR mode using a Nicolet iS50 spectrometer (Thermo Fisher Scientific, Waltham, MA, USA) with a resolution of 4 cm^{-1} at wavenumbers in the range of 500–4000 cm^{-1}. XRD patterns were collected at room temperature using the X-ray powder diffractometer MiniFlex600 by (RIGAKU, Tokyo, Japan). The experiments were carried out at 40 kV, 15 mA, with a filtered CuKα radiation λ = 1.54056 Å. The diffraction patterns were collected within the 2θ range of 18–70° with a step of 0.02°. The crystalline phase identification was performed with the application of Crystallography Open Database (COD).

3. Results and Discussion

3.1. Effect of HA Content, Temperature, and Depressurization Rate on PCL Foams Morphology

PCL films with different HA contents (10 and 20 wt.%) were prepared by solvent casting, as was described in Section 2.2. Figure 3 shows both sides of a film containing HA at 10%. As is visible in Figure 3b, the lower side of the film was smooth, indicating that HA particles were well dispersed and did not precipitate at the bottom during solvent removal.

The different PCL films were submitted to $scCO_2$-assisted foaming as described in Section 2.3 to evaluate the effect of temperature, HA content, and depressurization type on the scaffolds' final morphology. CO_2 saturation pressure was fixed at 20 MPa based on previously published results [45]. Figure 4 shows the images from the view cell during PCL foaming at 50 °C with a two-step decompression.

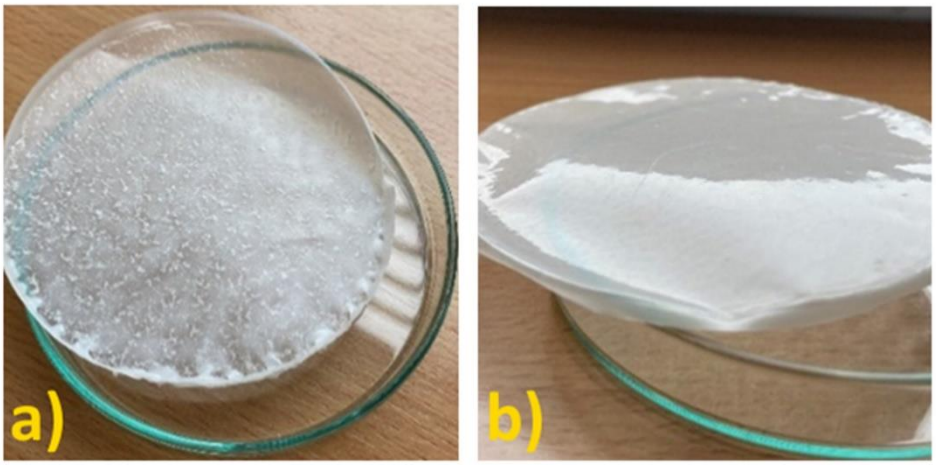

Figure 3. Polycaprolactone-hydroxyapatite (PCL-HA) 10 film after drying in the oven: (**a**) upper side; (**b**) lower side.

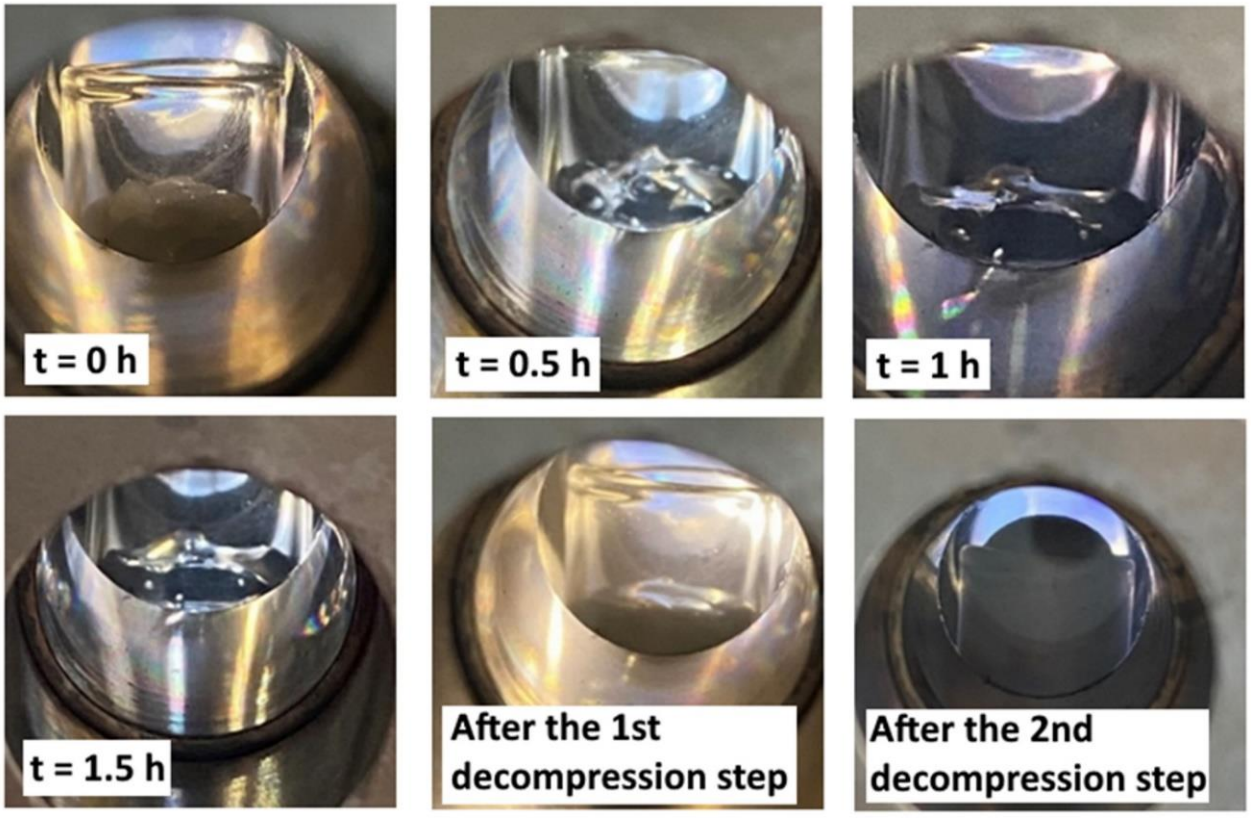

Figure 4. Progression of the sc-CO_2 assisted foaming of pure PCL at 50 °C and using a two-step decompression.

As can be seen, PCL granules were gradually melted during $scCO_2$ exposure at 50 °C until reaching a molten viscous state. After 1.5 h of $scCO_2$ exposure, a two-step decompression was performed at two different rates: from 20 to 9 MPa, the decompression rate was 0.5 MPa/min, from 9 MPa to ambient pressure, the decompression rate was 20 MPa/min. After the fast decompression, the foam was formed (Figure 4). Fanovic et al. [17] and Ivanovic et al. [20] reported melting temperatures ranging from 35 to 36 °C for pure PCL and PCL-HA composites as a function of HA concentrations (10–20 wt.%) exposed to $scCO_2$ at 17 MPa. Thus, in our study, the molten polymer state due to $scCO_2$ exposure was guaranteed for the assays done at both temperatures (40 and 50 °C) independent of the HA content in PCL films (0, 10 or 20 wt.%).

Table 1 and Figure 5 present the main morphological properties (porosity and density) and the results on the pore size distribution of the PCL scaffolds as a function of temperature, HA content, and depressurization type, respectively. These results show that temperature affected the final density of the PCL scaffolds independently of the HA content and the depressurization type used. At the lowest used temperature (40 °C) the obtained PCL scaffolds reached the lowest densities (Table 1). This fact could be explained in terms of the different CO_2 sorption in the polymeric structures as a function of the soaking temperature. Ivanovic et al. [20] reported that at constant pressure, the amount of CO_2 sorbed in PCL decreased as temperature increased due to the decrease in CO_2 density. Thus, in our study, a higher CO_2 sorption in PCL was expected using CO_2 at 40 °C due to its higher density compared with the density value at 50 °C. Thus, at 40 °C PCL presented lower viscosity which favored the nucleation rate. Consequently, at 40 °C the porosity of each PCL scaffold was higher, and therefore, their density was lower.

Table 1. Foam density and porosity of the neat and hydroxyapatite (HA) containing polycaprolactone (PCL) scaffolds obtained at different temperature and decompression rates.

Sample	HA (wt.%)	T (°C)	P (MPa)	t (h)	$\frac{dP}{dt}$ (MPa/min)	ρ_{foam} (g/cm^3)	ε (%)
PCL50	0	50	20	1.5	0.5; 20	0.3747	67.13
PCL50	0	50	20	1.5	0.5	0.8241	27.71
PCL-HA$_{10}$-50	10	50	20	1.5	0.5; 20	0.4739	64.68
PCL-HA$_{20}$-50	20	50	20	1.5	0.5; 20	0.5869	61.98
PCL40	0	40	20	1.5	0.5	0.2919	74.39
PCL40	0	40	20	1.5	0.5; 20	0.3593	64.07
PCL-HA$_{10}$-40	10	40	20	1.5	0.5	0.3953	70.54
PCL-HA$_{20}$-40	20	40	20	1.5	0.5	0.5319	65.55

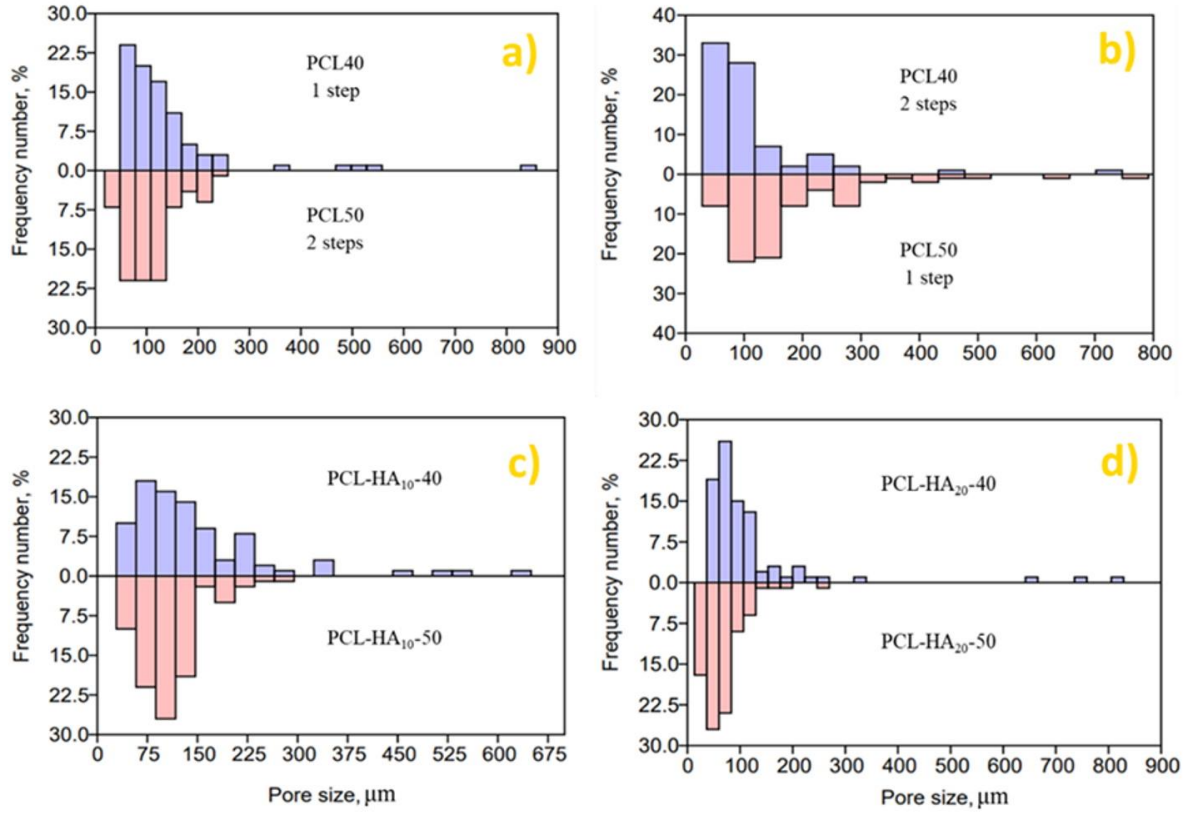

Figure 5. Pore size distribution of the PCL scaffolds as a function of temperature, HA content and decompression type; neat PCL (**a**,**b**), PCL with 10% HA (**c**), PCL with 20% HA (**d**).

Pure cast PCL films were used to evaluate the effect of depressurization type at different temperatures on the scaffolds' final morphology. The porosity and pore size distribution of the neat PCL scaffolds at different depressurization types and temperatures were reported in Table 1 and Figure 5, respectively. Meanwhile, Figure 6 shows the effect of decompression type on the morphology of neat PCL scaffolds obtained at 40 and 50 °C.

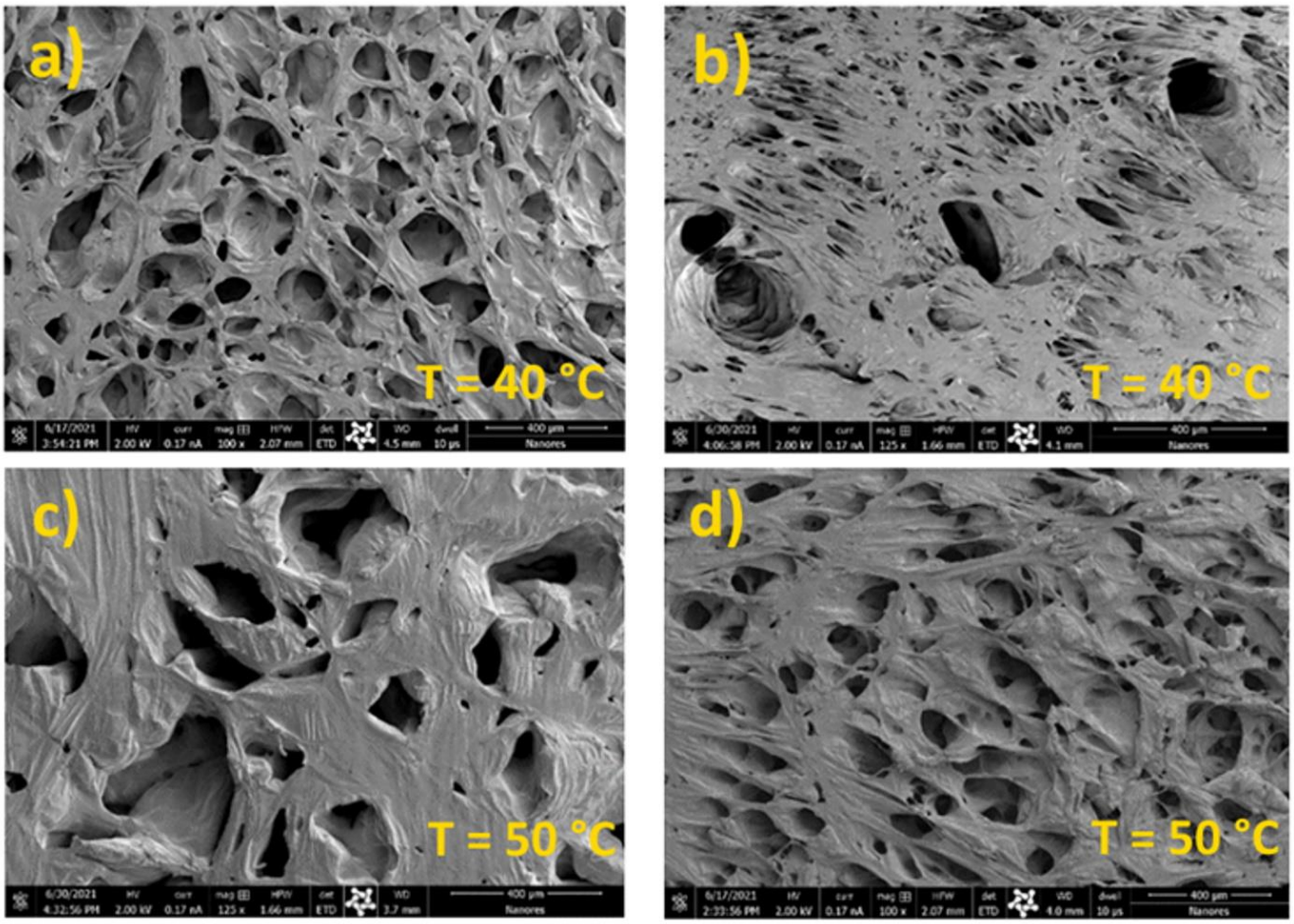

Figure 6. Effect of decompression type on the morphology of the neat PCL at T = 40 °C (**a**,**b**) and T = 50 °C (**c**,**d**): (**a**,**c**) one-step decompression; (**b**,**d**) two-step decompression.

At 40 °C, the neat PCL scaffold obtained using a two-step depressurization presented a broader pore size distribution with a larger number of small pores than the scaffold obtained using a one-step depressurization (Figure 5a,b), including a number of large size pores. Given that each depressurization step (slow and fast) encourages the formation of pores with different sizes, the two-step decompression generated a PCL foam with a bimodal distribution of pore sizes (Figure 6b) [42,46]. Particularly, the slow depressurization (0.5 MPa/min) allowed the formation of pores with larger sizes compared to the ones obtained with the fast depressurization (20 MPa/min), because it endows longer times for pores to grow and coalesce. Moreover, the mean pore size of the neat PCL scaffold decreased from 50 to 25 µm when depressurization type was changed from a one-step to a two-step depressurization showing that the mean pore size of the neat PCL scaffold was mainly determined by the second fast depressurization. The depressurization rate is one of the parameters that govern nucleation, where faster depressurization rates lead to higher degrees of nucleation [47]. This event facilitates CO_2 supersaturation, which improves nucleation and pore growth restriction leading to the formation of pores with smaller diameters and foams with higher porosity than the obtained using a slow depressurization. Interestingly, in our study, the porosity of the neat PCL scaffold was decreased from 74.39 to

64.07% when depressurization was changed from a one-step to a two-step depressurization. This result evidenced that the effect of the depressurization rate on the nucleation also depends on the amount of CO_2 sorbed in the polymer structure, which certainly was lower at 9 MPa than at 20 MPa. At 50 °C, the neat PCL scaffolds presented the opposite trend and had much higher porosity at a two-step depressurization, as can be seen in Table 1 and SEM images shown in Figure 6d. Based on the presented results, in further study with PCL–HA composites, the one-step decompression was selected for processing at 40 °C, while the two-step decompression was applied in experiments at 50 °C.

Figure 7 illustrates the morphology of the scaffolds obtained from PCL films with different HA contents at 40 °C (Figure 7a,c,e) using the one-step decompression and 50 °C (Figure 7b,d,f) using the two-step decompression. From these images, it can be seen that at the higher temperature the PCL scaffolds presented a slightly narrower pore size distribution compared with the values for the scaffolds obtained at the lower temperature (Figure 5c,d). However, PCL scaffolds obtained at 50 °C presented collapsed and non-uniform pores. This phenomenon has been related to the PCL phase coalescing before the crystallization of the polymeric matrix due to the use of temperatures well above the melting temperature of PCL [37].

Several studies have reported that parameters such as filler size and concentration have a strong impact on the morphology, porosity, and size pore distribution of porous materials [48,49]. In our study, the neat PCL scaffolds reached higher porosity values compared with the obtained for the PCL-HA scaffolds independently of the used temperature. This effect has been previously reported for PCL-HA composites produced through foaming processes based on different phenomena such as solvent [17] or non-solvent induced techniques [50]. Particularly, as the HA content increases, the PCL mass for pore formation decreases. Moreover, the composite system becomes denser as the HA content increases, which decreases the CO_2 mass transfer and its sorption in the composite polymer, which certainly makes the foaming process more difficult [51]. Thus, at 40 °C the highest porosity value was obtained for the neat PCL scaffold (74.39%). A similar porosity value for PCL has been previously reported by Ivanovic et al. [20] using similar $scCO_2$-assisted foaming conditions. At 40 °C, the porosity values for the composite PCL–HA_{10} and PCL–HA_{20} were 70.54% and 65.55%, respectively (Table 1).

These values were higher than the obtained at 50 °C. The effect of temperature on porosity was explained above. Thus, at 50 °C the porosity values for the PCL–HA_{10} and PCL–HA_{20} composites were 64.68% and 61.98%, respectively (Table 1). The HA content certainly influenced the effect of temperature on the pore size distribution of the scaffolds. The mean pore size of neat PCL and PCL–HA_{10} scaffolds decreased when temperature increased, conversely, PCL–HA_{20} scaffold had an opposite behavior due to the high content of HA. Meanwhile, closer pore size distributions were obtained as HA content was increased independent of temperature.

3.2. Effect of HA Content, Temperature, and Depressurization Rate on Carvacrol Loaded PCL Foams Morphology

PCL scaffolds loaded with carvacrol were obtained by a simultaneous $scCO_2$ assisted foaming and impregnation process as described in Section 2.3 to evaluate the effect of carvacrol addition on the scaffold's final morphology. Thus, the simultaneous foaming and impregnation assays were developed considering the same temperature values (40 and 50 °C) and HA contents (0, 10, and 20 wt.%) used to obtain the non-impregnated scaffolds, but using the previously selected decompression type for each temperature: the one-step decompression for processing at 40 °C, while the two-step decompression for the experiments at 50 °C. The obtained impregnation yields of carvacrol in the different PCL scaffolds are presented in Table 2.

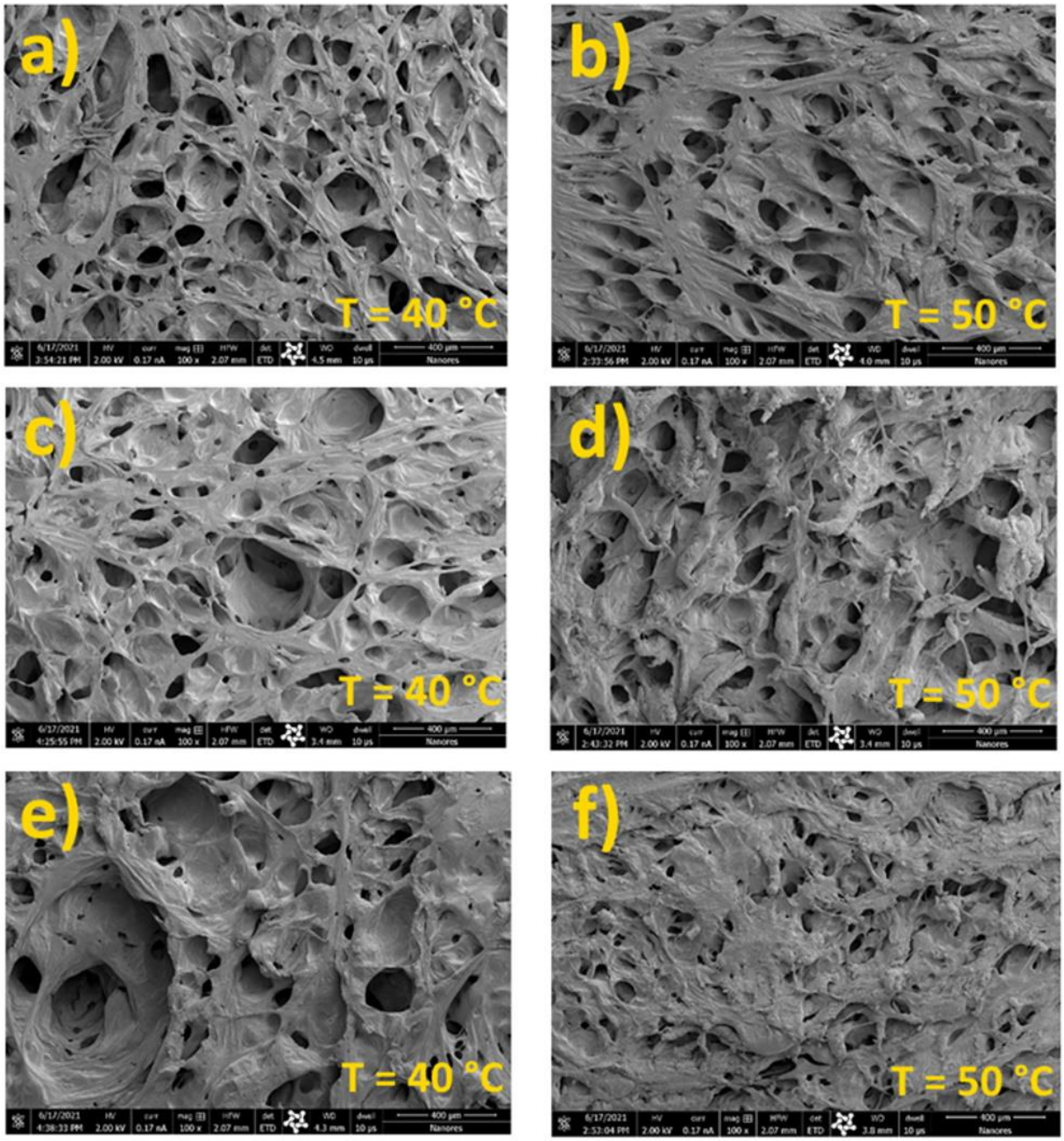

Figure 7. Scanning electron microscopy (SEM) micrographs of the neat PCL scaffold (**a**,**b**) and composite PLA scaffolds with different HA contents: 10 wt.% HA (**c**,**d**) and 20 wt.% HA (**e**,**f**) obtained at different temperatures.

Table 2. Foam density, porosity and carvacrol impregnation yield of the impregnated PCL scaffolds with different HA contents obtained at different temperatures and decompression rates.

Sample	HA (%)	T (°C)	P (MPa)	$\frac{dP}{dt}$ (MPa/min)	ρ_{foam} (g/cm^3)	ε (%)	Impregnation Yield (wt.%)
PCL50	0	50	20	0.5; 20	0.5926	48.01	7.22
PCL-HA$_{10}$-50	10	50	20	0.5; 20	0.6835	49.07	10.57
PCL-HA$_{20}$-50	20	50	20	0.5; 20	0.8077	47.69	10.24
PCL40	0	40	20	0.5	0.3724	67.33	7.71
PCL-HA$_{10}$-40	10	40	20	0.5	0.4951	63.11	10.41
PCL-HA$_{20}$-40	20	40	20	0.5	0.7225	53.21	9.27

To our knowledge, this is the first study on the simultaneous supercritical foaming and impregnation of carvacrol in composite PCL scaffolds. In addition, there is no previous information about the supercritical impregnation of carvacrol in PCL-based polymeric structures. Overall, satisfactory impregnation yields (7.22–10.57 wt.%) were achieved for all the samples at the studied conditions. Nevertheless, these impregnation yields were lower than the reported for carvacrol in other polymers such as cellulose acetate films (31 wt.%) [52] and polyamide membranes (40 wt.%) [53] using similar processing conditions, which evidence the low chemical affinity between carvacrol and PCL. Interestingly, the reported impregnation yield of thymol (14.8 wt.%) in pure PCL [20] was considerably higher than the obtained in this study for carvacrol in the pure PCL scaffolds using very similar processing conditions (7.22–7.71 wt.%), even considering the great chemical similarity between both phenolic compounds. Thymol and carvacrol are position isomers because their chemical structures only differ in the spatial orientation of the hydroxyl group on the aromatic ring. Thus, the relative position of the hydroxyl group on the aromatic ring of carvacrol and thymol may have influenced their different affinities towards PCL. This fact could also influence the different impregnation yields reported for carvacrol (21.2 wt.%) and thymol (27.5 wt.%) in PLA films at the same processing conditions [54]. Moreover, the carvacrol impregnation yield was increased due to the HA addition to PCL at both combinations of temperature and decompression type (Table 2). This result is very interesting because the reported impregnation yield of thymol in PCL/HA composite scaffolds decreased as the HA content increased from 10 to 20 wt.% as reported by Ivanovic [20]. In this way, the different affinities of both phenolic compounds towards HA could also be related to the relative position of the hydroxyl group on the aromatic ring of carvacrol and thymol. In this work, the HA content variation (10 and 20 wt.%) seems to have a negligible influence on the carvacrol impregnation yield (~3.1%) at both combinations of temperature and decompression type (Table 2).

The PCL-HA_{10}-50 scaffold with the highest impregnation yield was investigated by the Fourier-Transform Infrared (FTIR) analyses (Figure 8) to confirm the presence of carvacrol. A spectrum of neat PCL-HA_{10}-50 scaffold was also presented for comparison. Both spectra show a peak around 2800–3000 cm^{-1} and a very sharp signal at 1750 cm^{-1} corresponding to alkyl chains and ester groups of PCL, respectively [55]. New peaks appeared in the FTIR spectrum of the impregnated PCL scaffold, which indicated the carvacrol presence. New peaks in the range of 1580–1620 cm^{-1} are assigned for stretching C=C bond in the aromatic ring of carvacrol. The peaks that appeared in the range of 800–810 cm^{-1} show the presence of C-H out-of-plane wagging bonds. Moreover, peaks in the range 995–990 cm^{-1} confirm 1:2:4-Substituion of carvacrol [56].

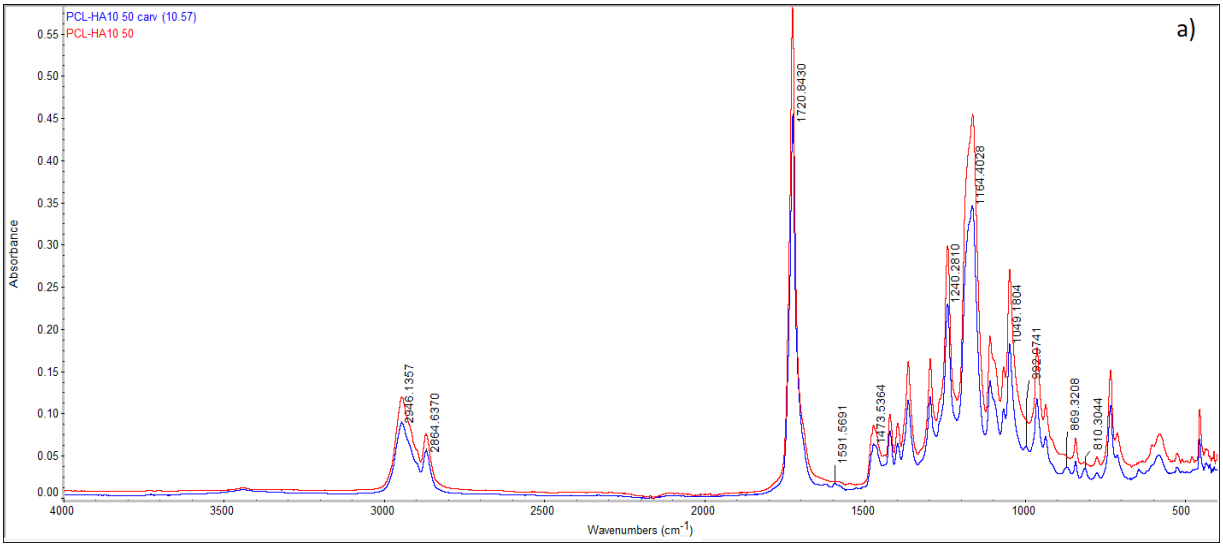

Figure 8. *Cont.*

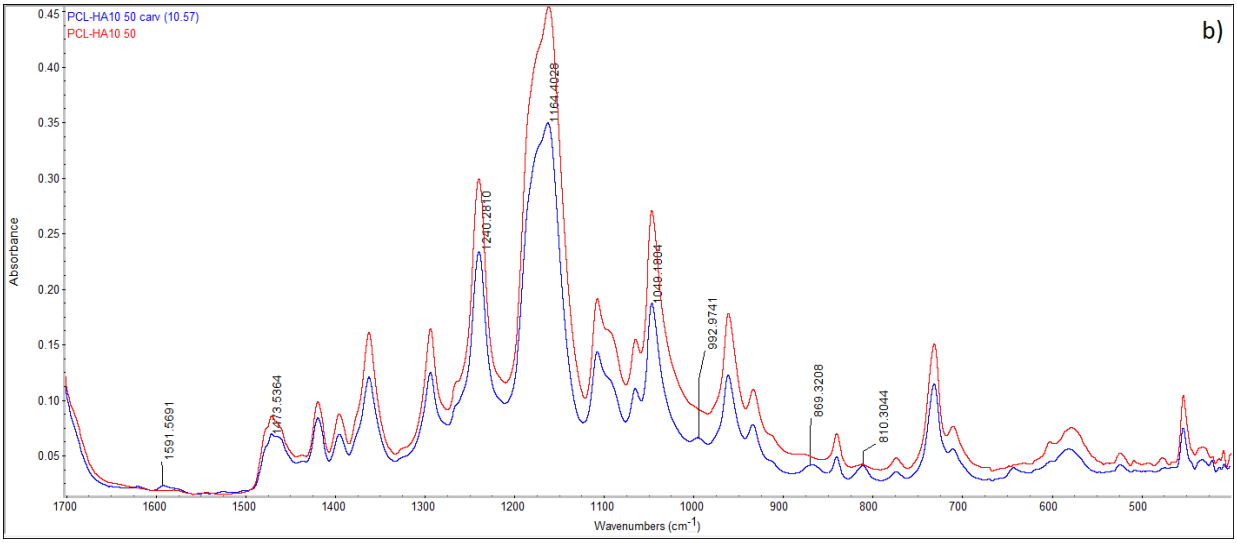

Figure 8. Fourier-transform infrared (FTIR) spectra of the PCL-HA_{10}−50 (red) and impregnated with carvacrol PCL-HA_{10}−50 scaffold (blue): (**a**) full spectra; (**b**) part of the spectrum with characteristic carvacrol's peaks.

FTIR analysis was also used to confirm the presence of HA in the composite foams. Spectra of the neat PCL scaffold and scaffold with 20% HA PCL-HA_{20}-50 are presented in Figure 9. New intensive bands appearing in the spectrum of the composite scaffold at 570 and 600 cm^{-1}, and at 1000–1100 cm^{-1} originate from PO_4^{3-} group [57].

The presence of HA is also visible in XRD patterns of PCL foam and PCL scaffolds with 20% of HA obtained at 50 °C (Figure 10). The phases detected were both PCL and hydroxyapatite HA. The characteristic diffraction peaks are marked for the observed phases (Figure 10). The PCL sample exhibited relatively strong intensity peaks visible at 2 theta of 21.77° and 24.08°, corresponding to the (110) and (200) Bragg reflections. For samples with HA, new peaks were observed of lower intensity. However, there were no significant differences in patterns of samples with 20% HA with and without carvacrol.

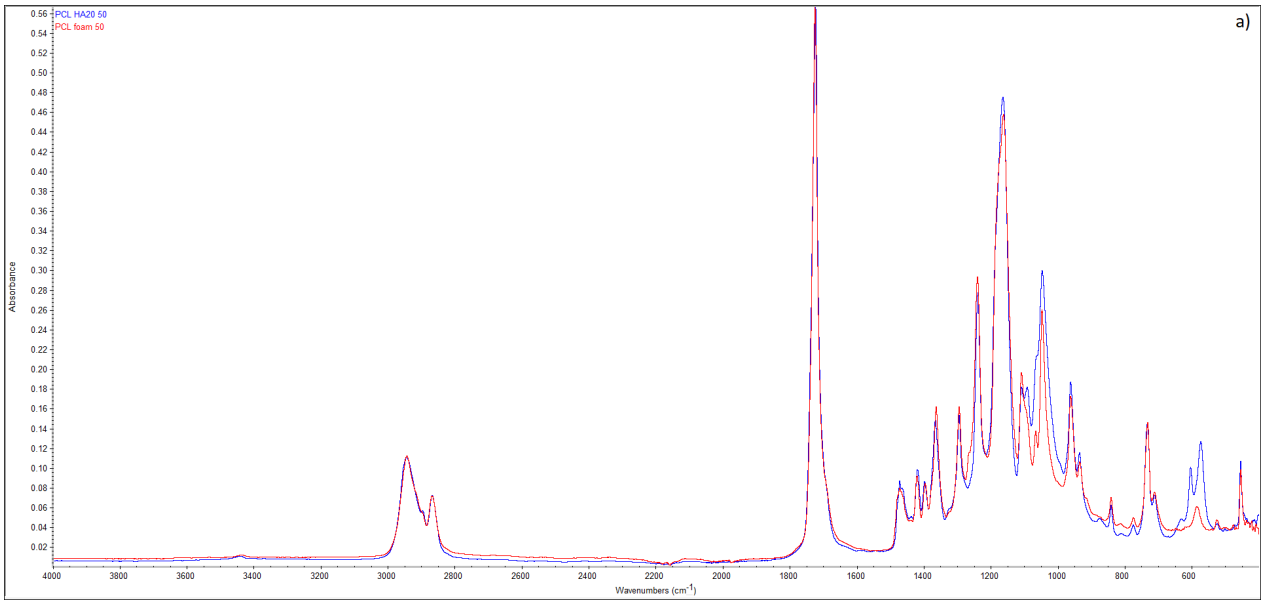

Figure 9. *Cont.*

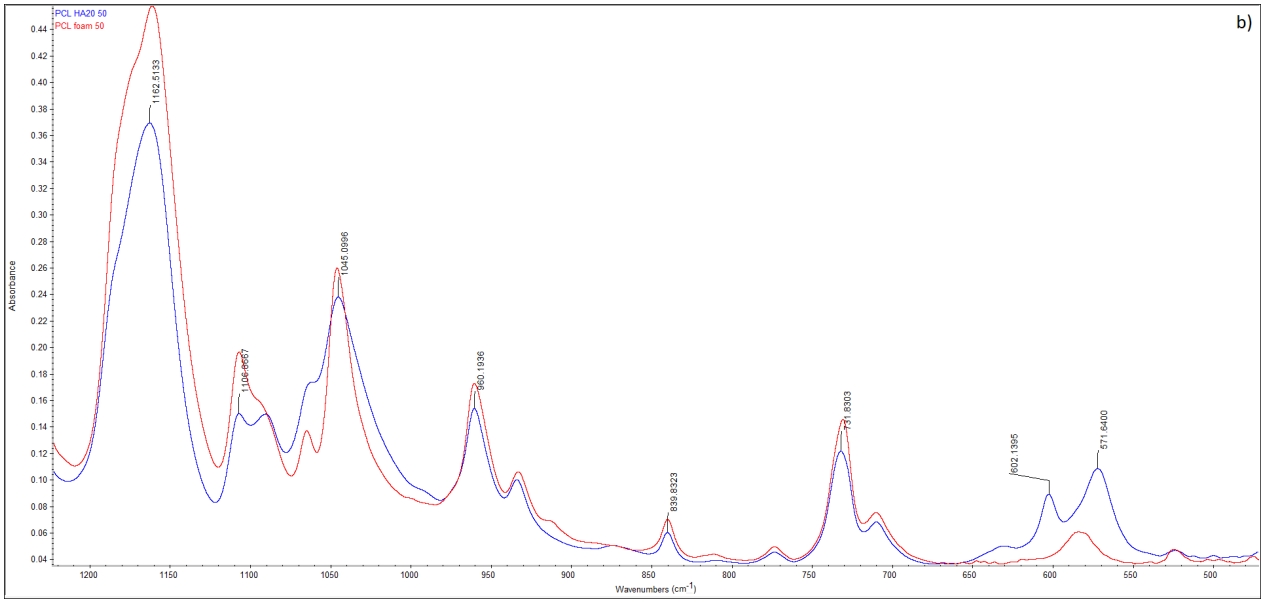

Figure 9. Fourier-transform infrared (FTIR) spectra of the PCL scaffold (red) and PCL-HA_{20}-50 scaffold (blue): (**a**) full spectra; (**b**) part of the spectrum with characteristic peaks of HA.

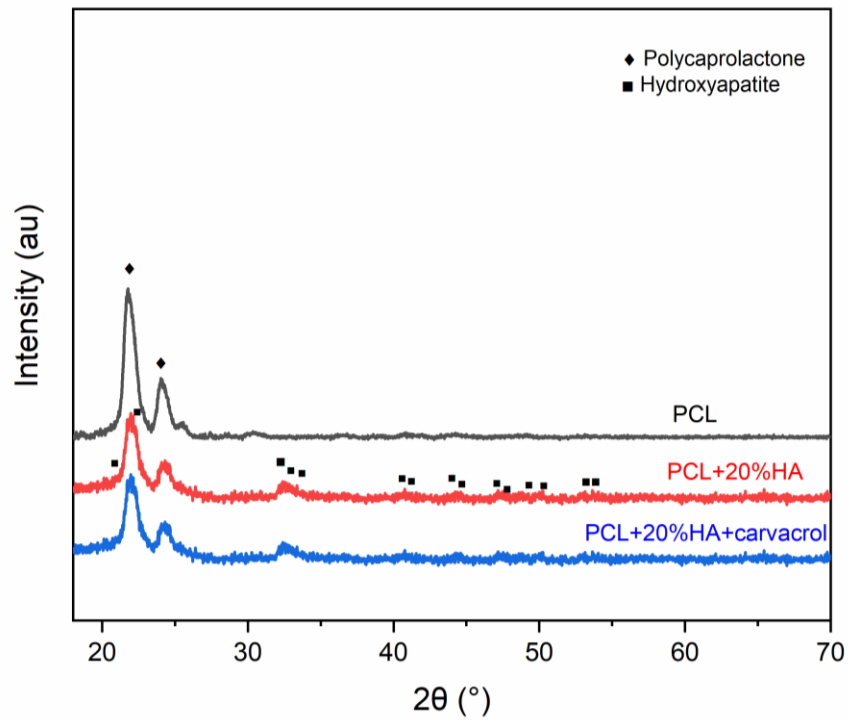

Figure 10. X-ray diffraction (XRD) patterns of PCL and PCL-HA_{20}-50 scaffolds.

Table 2 shows that the carvacrol impregnation yield was practically independent of the different temperature and decompression type combinations used in this work. Obviously, this fact should response to a combined effect of temperature and decompression type used in both processing conditions. Regarding temperature, this factor could have a small influence on the amount of carvacrol impregnated in the PCL scaffolds because the solubility of carvacrol in CO_2 at 40 °C is only slightly higher than the solubility reported at 50 °C using pressures near to 20 MPa [58], which established at both processing conditions a similar carvacrol concentration gradient. This fact could also be related with the negligible influence of temperature (35–40 °C) at 17 MPa over the impregnation yield reported

for thymol in PCL [20]. Moreover, the positive effect of the slightly higher carvacrol concentration gradient at 40 °C on the thymol impregnation yield could be counterbalanced by the higher carvacrol diffusion coefficient at 50 °C. Regarding decompression, this is one of the main factors which governs the impregnation yield. According to theory, for polymer systems with low affinity towards an impregnating substance the impregnation yield is generally favored using a fast decompression, unlike for systems with high affinity to the impregnating substance a slow decompression could induce the higher impregnation yield [12]. Particularly, slow decompression rates have been related with higher carvacrol impregnation yield in cellulose acetate [52]. Based on this statement, a significantly higher carvacrol impregnation yield should have been obtained using the slow decompression step instead of the fast decompression. Nevertheless, both processing conditions begin with a slow-step decompression (0.5 MPa/min) from 20 to 9 MPa, which allows us to hypothesize that carvacrol was mainly incorporated in the PCL structure during the first slow-step decompression as the molten polymer begins to solidify.

On the other hand, temperature and decompression type influenced the porosity values of the PCL scaffolds in the same way that was observed for the non-impregnated scaffolds. Thus, the impregnated PCL foam obtained at 40 °C and using the one-step decompression presented a higher porosity than the obtained using 50 °C and the two-step decompression. Moreover, the porosity of the scaffolds decreased due to the carvacrol impregnation (Table 2). This fact could be explained in terms of the CO_2 sorption decrease in the PCL structure during the CO_2 saturation stage due to the presence of carvacrol in the supercritical phase. The carvacrol presence reduced the number of CO_2 molecules able to be sorbed in PCL, and the sites in the PCL structure able to interact with them due to carvacrol absorption, generating a lower nucleation rate than in the experiments done with pure CO_2 (Table 1).

Carvacrol incorporation into the polymer scaffolds at 40 °C did not considerably affect their pore size distribution compared with the non-impregnated PCL scaffolds (Figures 5 and 11). However, for the samples PCL and PCL-HA_{20} obtained at 50 °C, a larger fraction of smaller pores was detected in the presence of carvacrol (Figures 5 and 10), as also visible in SEM images presented in Figures 7 and 12. Moreover, the scaffolds' porosity decrease seems to be independent of the amount of carvacrol impregnated in their structures (see Table 2). Impregnated neat PCL scaffolds obtained at 40 °C and 50 °C reached similar carvacrol loadings, 7.71 and 7.22 wt.%, but very different porosity values, 67.33 and 48.0%, respectively, showing that PCL porosity was highly governed by the decompression type. Particularly, the second fast decompression for the simultaneous impregnation and foaming experiments performed at 50 °C could be the main factor associated with the significant decrease in porosity (Table 2) and mean size pore diameter (Figure 11) of the impregnated scaffolds with respect to the porosity (Table 1) and mean pore diameter (Figure 5) of the non-impregnated scaffolds. Interestingly, the scaffolds obtained at 50 °C and the two-step decompression reached porosity values practically independent of carvacrol and HA content. Although the impregnated PCL-HA scaffolds presented a higher amount of carvacrol (10.24–10.57 wt.%) than the neat PCL scaffold (7.22 wt.%) the samples had closed porosity values ranging between 47.69 and 49.07%. This result reinforces the hypothesis that PCL porosity was mainly controlled by the second fast decompression. In the opposite way, at 40 °C and using the one-step decompression, the scaffolds' porosity slightly decreased due to the carvacrol impregnation maintaining the effect of HA content on scaffolds' porosity evidenced in the foaming assays done without carvacrol. Thus, at 40 °C and using the slow one-step decompression the lowest porosity (53.21%) was obtained for the PCL scaffolds with the higher HA content (Table 2). Also, the average pore size of non-impregnated PCL-HA scaffolds was only slightly decreased compared to the impregnated scaffolds obtained at the same conditions, 133 μm and 140 μm, respectively. Ivanovic et al. [20] have also reported that the average pore diameters of the composite foam impregnated with thymol and non-impregnated composite foam were practically the same (at 40 °C, 17 MPa, and decompression rate of 0.5 MPa/min).

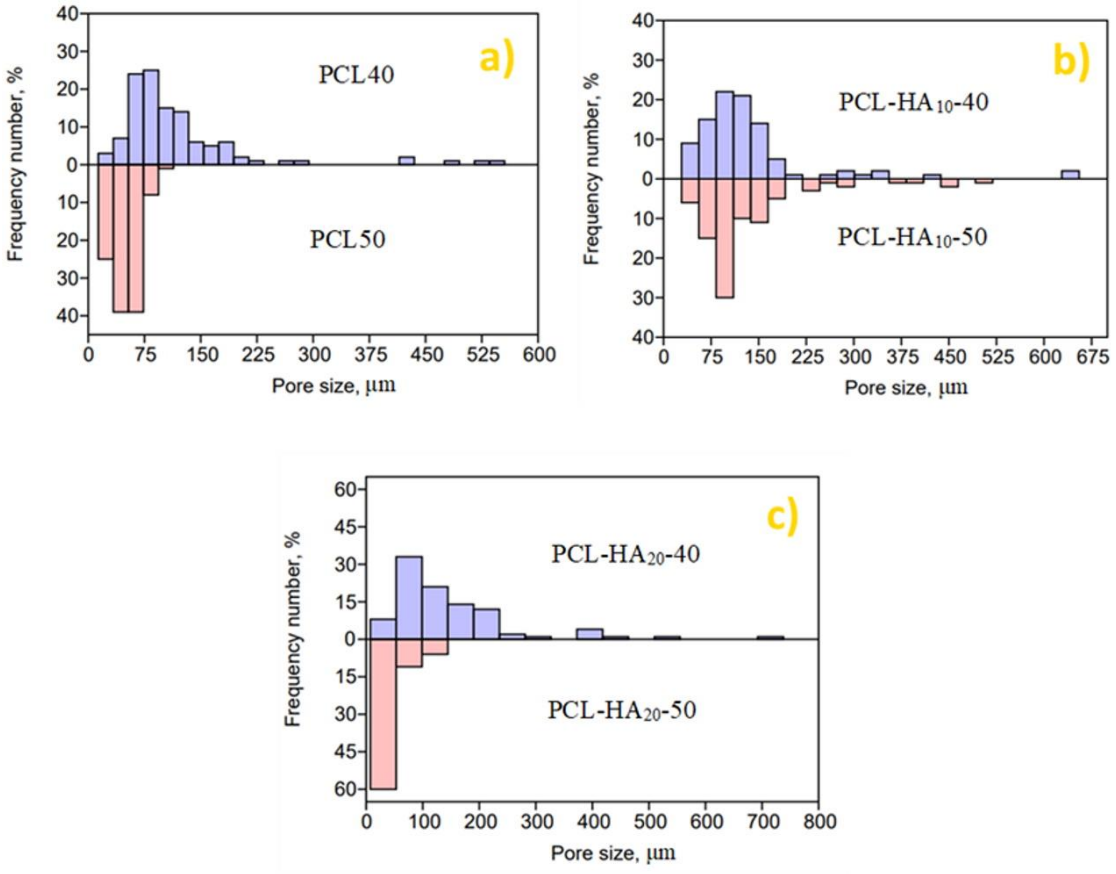

Figure 11. Pore size distribution of the PCL scaffolds after impregnation with carvacrol: neat PCL (**a**), PCL with 10% HA (**b**), PCL with 20% HA (**c**).

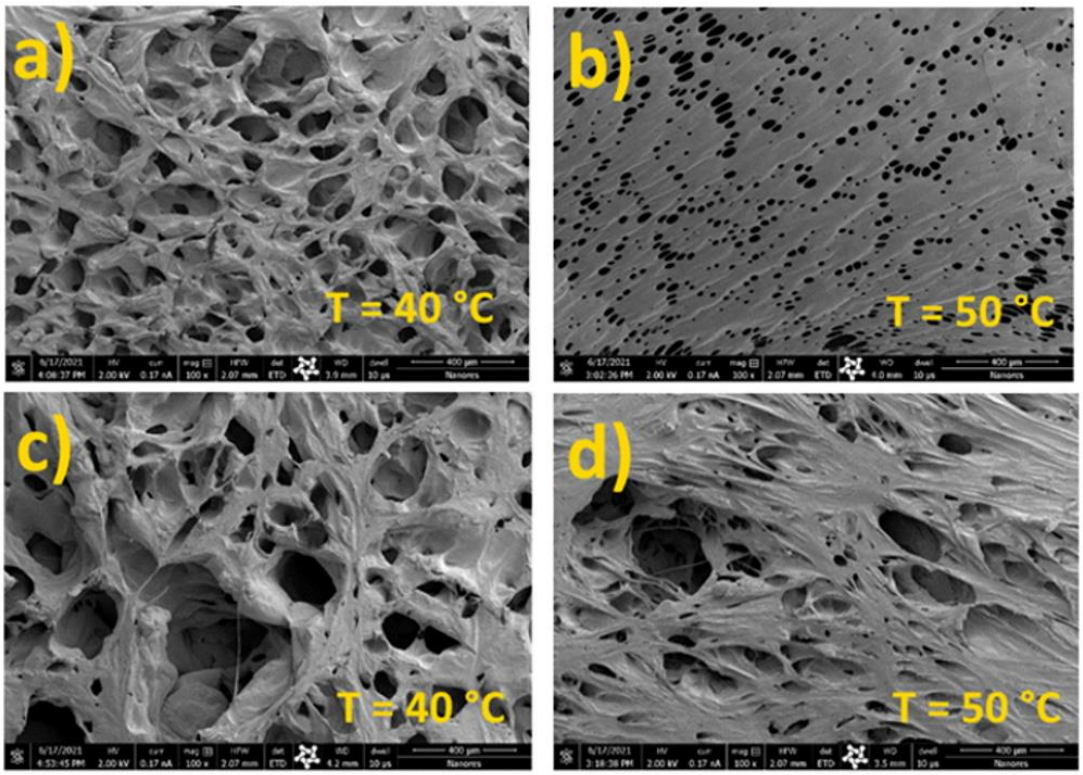

Figure 12. *Cont.*

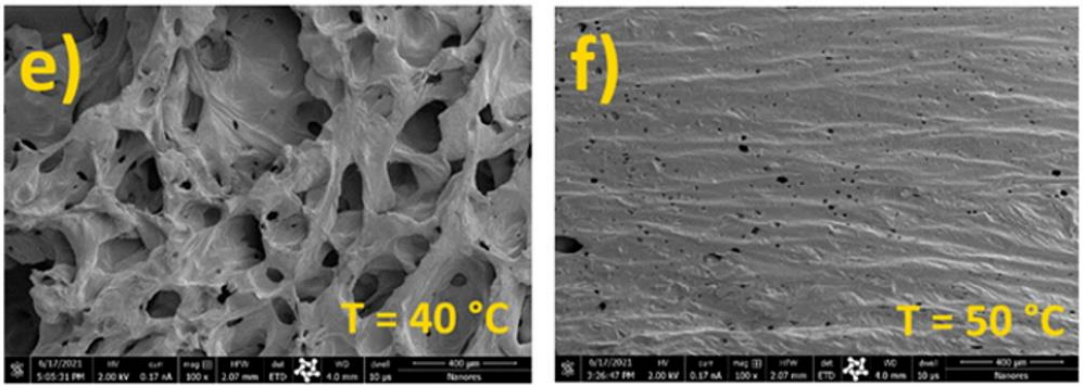

Figure 12. Effect of the impregnation with the carvacrol on the morphology of the neat PCL (**a**,**b**), PCL-HA_{10} (**c**,**d**) and PCL-HA_{20} (**e**,**f**).

The mechanical properties of scaffolds were screened by measuring the compression force to induce deformation (Appendix B). These preliminary results (Table A2, Appendix B) indicate that foams with 20% HA were the most sensitive to compression stress.

4. Conclusions

This work aimed to investigate the foaming and impregnation with carvacrol of PCL and PCL-HA composites using $scCO_2$. The effect of temperature, decompression type, and HA content on the morphology and carvacrol impregnation yield was studied. The scaffolds synthesized at a higher temperature (T = 50 °C) and using the two-step fast decompression presented a narrower pore size distribution. However, a higher porosity was achieved for the scaffolds obtained at the lower temperature (T = 40 °C) and using the one-step slow decompression rate. At 40 and 50 °C, the range of scaffolds' porosity was 65.55–74.39% and 61.98–67.13%, respectively. The porosity results for the carvacrol loaded PCL showed the same trend with the porosity in the range of 53.21–67.33% and 47.69–49.07%, at 40 °C and 50 °C, respectively. The presence of carvacrol decreased the scaffolds' porosity. PCL scaffolds with HA resulted in higher impregnation yields than neat PCL scaffolds, 9.27–10.57 wt.% and 7.22–7.71 wt.%, respectively. The highest porosity and carvacrol impregnation yield was achieved for the scaffolds with 10 wt.% of HA (10.57 wt.%) obtained at 50 °C. The study results demonstrated the feasibility of the one-step foaming and impregnation process for the production of carvacrol-loaded PCL-based scaffolds. The results also demonstrated that different decompression types were needed to obtain desired porosity at different temperatures. The two-step fast decompression was required to obtain a high porosity at 50 °C.

Author Contributions: Conceptualization, A.S., I.Z. and A.R.; methodology, A.S. and I.Z.; validation, I.Z. and A.R.; investigation, A.S., M.T., E.K. and I.Z.; resources I.Z. and M.J.G.; writing—original draft preparation, A.S., A.R. and I.Z.; writing—review and editing, A.R., I.Z. and M.J.G. All authors have read and agreed to the published version of the manuscript.

Funding: The research was funded by Narodowe Centrum Nauki, (Poland), grant number 2018/31/B/ST8/01826. The financial support is gratefully acknowledged. M.J.G and A.R. thanks the support of Agencia Nacional de Investigación y Desarrollo through the Fondecyt regular project N°1201301 and to the the "Programa de Financiamiento Basal para Centros Científicos y Tecnológicos de Excelencia" (Project AFB180001).

Conflicts of Interest: The authors declare no conflict of interest.

Appendix A

Table A1. Summarized experimental conditions.

Sample	HA (wt.%)	T (°C)	P (MPa)	t (h)	One-Step Decompression (MPa/min)	Two-Step Decompression (MPa/min)
FOAMING						
PCL50	0	50	20	1.5		0.5; 20
PCL50	0	50	20	1.5	0.5	
PCL-HA_{10}-50	10	50	20	1.5		0.5; 20
PCL-HA_{20}-50	20	50	20	1.5		0.5; 20
PCL40	0	40	20	1.5	0.5	
PCL40	0	40	20	1.5		0.5; 20
PCL-HA_{10}-40	10	40	20	1.5	0.5	
PCL-HA_{20}-40	20	40	20	1.5	0.5	
FOAMING AND IMPREGNATION						
PCL50	0	50	20	3		0.5; 20
PCL-HA_{10}-50	10	50	20	3		0.5; 20
PCL-HA_{20}-50	20	50	20	3		0.5; 20
PCL40	0	40	20	3	0.5	
PCL-HA_{10}-40	10	40	20	3	0.5	
PCL-HA_{20}-40	20	40	20	3	0.5	

Appendix B

The scaffolds' mechanical properties were screened by measuring the compression force that caused foams deformation using IMADA Force Gauge with stand MX2-500N (IMADA. CO. LTD, Aichi, Japan). The results are presented in Table A2. The data indicated that samples containing 20% HA were the most sensitive to compression stress.

Table A2. The compression force to start deformation of neat (F_{NEAT}) and impregnated (F_{IMPREG}) scaffolds.

Sample	F_{NEAT} (N)	F_{IMPREG} (N)
PCL50	53.2	51.3
PCL-HA_{10}-50	52.4	51.4
PCL-HA_{20}-50	35.6	32.9
PCL40	42.5	46.1
PCL-HA_{10}-40	36.2	38.6
PCL-HA_{20}-40	34.3	29.1

References

1. Wu, A.-M.; Bisignano, C.; James, S.L.; Abady, G.G.; Abedi, A.; Abu-Gharbieh, E.; Alhassan, R.K.; Alipour, V.; Arabloo, J.; Asaad, M.; et al. Global, Regional, and National Burden of Bone Fractures in 204 Countries and Territories, 1990–2019: A Systematic Analysis from the Global Burden of Disease Study 2019. *Lancet Healthy Longev.* **2021**, *2*, e580–e592. [CrossRef]
2. Dimitriou, R.; Jones, E.; McGonagle, D.; Giannoudis, P.V. Bone Regeneration: Current Concepts and Future Directions. *BMC Med.* **2011**, *9*, 1–10. [CrossRef] [PubMed]
3. Soucacos, P.N.; Johnson, E.O.; Babis, G. *An Update on Recent Advances in Bone Regeneration*; Elsevier: Amsterdam, The Netherlands, 2008; Volume 39.
4. Amini, A.R.; Laurencin, C.T.; Nukavarapu, S.P. Bone Tissue Engineering: Recent Advances and Challenges. *Crit. Rev. Biomed. Eng.* **2012**, *40*, 363–408. [CrossRef] [PubMed]
5. Tsang, V.L.; Bhatia, S.N. Fabrication of Three-Dimensional Tissues. *Adv. Biochem. Eng. Biotechnol.* **2006**, *103*, 189–205.
6. Dutta, R.C.; Dey, M.; Dutta, A.K.; Basu, B. Competent Processing Techniques for Scaffolds in Tissue Engineering. *Biotechnol. Adv.* **2017**, *35*, 240–250. [CrossRef]
7. Reverchon, E.; Cardea, S. Supercritical Fluids in 3-D Tissue Engineering. *J. Supercrit. Fluids* **2012**, *69*, 97–107. [CrossRef]
8. Duarte, A.R.C.; Mano, J.F.; Reis, R.L. Perspectives on: Supercritical Fluid Technology for 3D Tissue Engineering Scaffold Applications. *J. Bioact. Compat. Polym.* **2009**, *24*, 385–400. [CrossRef]

9. Davies, O.R.; Lewis, A.L.; Whitaker, M.J.; Tai, H.; Shakesheff, K.M.; Howdle, S.M. Applications of Supercritical CO_2 in the Fabrication of Polymer Systems for Drug Delivery and Tissue Engineering. *Adv. Drug Deliv. Rev.* **2008**, *60*, 373–387. [CrossRef]
10. Clifford, A.A.; Williams, J.R. Introduction to Supercritical Fluids and Their Applications. In *Supercritical Fluid Methods and Protocols*; Humana Press: Totowa, NJ, USA, 2000; Volume 13, pp. 1–16.
11. Champeau, M.; Thomassin, J.M.; Tassaing, T.; Jérôme, C. Drug Loading of Polymer Implants by Supercritical CO_2 Assisted Impregnation: A Review. *J. Control. Release* **2015**, *209*, 248–259. [CrossRef]
12. Rojas, A.; Torres, A.; Galotto, M.J.; Guarda, A.; Julio, R. Supercritical Impregnation for Food Applications: A Review of the Effect of the Operational Variables on the Active Compound Loading. *Crit. Rev. Food Sci. Nutr.* **2020**, *60*, 1290–1301. [CrossRef]
13. Chauvet, M.; Sauceau, M.; Baillon, F.; Fages, J. Blending and Foaming Thermoplastic Starch with Poly (Lactic Acid) by CO_2-aided Hot Melt Extrusion. *J. Appl. Polym. Sci.* **2021**, *138*, 50150. [CrossRef]
14. Tsivintzelis, I.; Sanxaridou, G.; Pavlidou, E.; Panayiotou, C. Foaming of Polymers with Supercritical Fluids: A Thermodynamic Investigation. *J. Supercrit. Fluids* **2016**, *110*, 240–250. [CrossRef]
15. Okamoto, M.; John, B. Synthetic Biopolymer Nanocomposites for Tissue Engineering Scaffolds. *Prog. Polym. Sci.* **2013**, *38*, 1487–1503. [CrossRef]
16. Jenkins, M.J.; Harrison, K.L.; Silva, M.M.C.G.; Whitaker, M.J.; Shakesheff, K.M.; Howdle, S.M. Characterisation of Microcellular Foams Produced from Semi-Crystalline PCL Using Supercritical Carbon Dioxide. *Eur. Polym. J.* **2006**, *42*, 3145–3151. [CrossRef]
17. Fanovich, M.A.; Ivanovic, J.; Zizovic, I.; Misic, D.; Jaeger, P. Functionalization of Polycaprolactone/Hydroxyapatite Scaffolds with Usnea Lethariiformis Extract by Using Supercritical CO_2. *Mater. Sci. Eng. C* **2016**, *58*, 204–212. [CrossRef]
18. Pitt, C.G.; Gratzl, M.M.; Kimmel, G.L.; Surles, J.; Schindler, K. Aliphatic Polyesters II. The Degradation of Poly (DL-Lace), Poly (E-Caprolactone), and Their Copolymers in Vivo. *Biomaterials* **1981**, *2*, 215–220. [CrossRef]
19. Choi, S.H.; Park, T.G. Synthesis and Characterization of Elastic PLGA/PCL/PLGA Tri-Block Copolymers. *J. Biomater. Sci. Polym. Ed.* **2002**, *13*, 1163–1173. [CrossRef]
20. Ivanovic, J.; Knauer, S.; Fanovich, A.; Milovanovic, S.; Stamenic, M.; Jaeger, P.; Zizovic, I.; Eggers, R. Supercritical CO_2 Sorption Kinetics and Thymol Impregnation of PCL and PCL-HA. *J. Supercrit. Fluids* **2016**, *107*, 486–498. [CrossRef]
21. Knowles, J.C. Phosphate Based Glasses for Biomedical Applications. *J. Mater. Chem.* **2003**, *13*, 2395–2401. [CrossRef]
22. Kim, H.W.; Knowles, J.C.; Kim, H.E. Hydroxyapatite Porous Scaffold Engineered with Biological Polymer Hybrid Coating for Antibiotic Vancomycin Release. *J. Mater. Sci. Mater. Med.* **2005**, *16*, 189–195. [CrossRef]
23. Puppi, D.; Dinucci, D.; Bartoli, C.; Mota, C.; Migone, C.; Dini, F.; Barsotti, G.; Carlucci, F.; Chiellini, F. Development of 3D Wet-Spun Polymeric Scaffolds Loaded with Antimicrobial Agents for Bone Engineering. *J. Bioact. Compat. Polym.* **2011**, *26*, 478–492. [CrossRef]
24. Aeschbach, R.; Loliger, J.; Scott, C.; Murcia, A.; Butler, J.; Aruoma, O.I. Antioxidant actions of thymol, carvacrol, 6-gingerol, zingerone and hydroxytyrosol. *Food Chem. Toxicol.* **1994**, *32*, 31–36. [CrossRef]
25. Chouhan, S.; Sharma, K.; Guleria, S. Antimicrobial Activity of Some Essential Oils—Present Status and Future Perspectives. *Medicines* **2017**, *4*, 58. [CrossRef] [PubMed]
26. Xu, J.; Zhou, F.; Ji, B.P.; Pei, R.S.; Xu, N. The Antibacterial Mechanism of Carvacrol and Thymol against *Escherichia Coli*. *Lett. Appl. Microbiol.* **2008**, *47*, 174–179. [CrossRef]
27. Nostro, A.; Papalia, T. Antonia Nostro; Teresa Papalia Antimicrobial Activity of Carvacrol: Current Progress and Future Prospectives. *Recent Pat. Anti-Infect. Drug Discov.* **2012**, *7*, 28–35. [CrossRef]
28. Nostro, A.; Blanco, A.R.; Cannatelli, M.A.; Enea, V.; Flamini, G.; Morelli, I.; Sudano Roccaro, A.; Alonzo, V. Susceptibility of Methicillin-Resistant Staphylococci to Oregano Essential Oil, Carvacrol and Thymol. *FEMS Microbiol. Lett.* **2004**, *230*, 191–195. [CrossRef]
29. U.S. Food & Drug Administration. *CFR—Code of Federal Regulations Title 21*; FDA: Silver Spring, MD, USA, 2012.
30. Zizovic, I. Supercritical Fluid Applications in the Design of Novel Antimicrobial Materials. *Molecules* **2020**, *25*, 2491. [CrossRef]
31. Milovanovic, S.; Markovic, D.; Aksentijevic, K.; Stojanovic, D.B.; Ivanovic, J.; Zizovic, I. Application of Cellulose Acetate for Controlled Release of Thymol. *Carbohydr. Polym.* **2016**, *147*, 344–353. [CrossRef]
32. Pajnik, J.; Lukić, I.; Dikić, J.; Asanin, J.; Gordic, M.; Misic, D.; Zizović, I.; Korzeniowska, M. Application of Supercritical Solvent Impregnation for Production of Zeolite Modified Starch-Chitosan Polymers with Antibacterial Properties. *Molecules* **2020**, *25*, 4717. [CrossRef]
33. Milovanovic, S.; Jankovic-Castvan, I.; Ivanovic, J.; Zizovic, I. Effect of Starch Xero- And Aerogels Preparation on the Supercritical CO_2 Impregnation of Thymol. *Starch Staerke* **2015**, *67*, 174–182. [CrossRef]
34. Kiran, E. Foaming Strategies for Bioabsorbable Polymers in Supercritical Fluid Mixtures. Part I. Miscibility and Foaming of Poly(l-Lactic Acid) in Carbon Dioxide + Acetone Binary Fluid Mixtures. *J. Supercrit. Fluids* **2010**, *54*, 308–319. [CrossRef]
35. Fanovich, M.A.; Jaeger, P. Sorption and Diffusion of Compressed Carbon Dioxide in Polycaprolactone for the Development of Porous Scaffolds. *Mater. Sci. Eng. C* **2012**, *32*, 961–968. [CrossRef]
36. Milovanovic, S.; Stamenic, M.; Markovic, D.; Ivanovic, J.; Zizovic, I. Supercritical Impregnation of Cellulose Acetate with Thymol. *J. Supercrit. Fluids* **2015**, *97*, 107–115. [CrossRef]
37. Salerno, A.; Zeppetelli, S.; di Maio, E.; Iannace, S.; Netti, P.A. Novel 3D Porous Multi-Phase Composite Scaffolds Based on PCL, Thermoplastic Zein and Ha Prepared via Supercritical CO_2 Foaming for Bone Regeneration. *Compos. Sci. Technol.* **2010**, *70*, 1838–1846. [CrossRef]

38. Salerno, A.; di Maio, E.; Iannace, S.; Netti, P.A. Solid-State Supercritical CO_2 Foaming of PCL and PCL-HA Nano-Composite: Effect of Composition, Thermal History and Foaming Process on Foam Pore Structure. *J. Supercrit. Fluids* **2011**, *58*, 158–167. [CrossRef]
39. Karageorgiou, V.; Kaplan, D. Porosity of 3D Biomaterial Scaffolds and Osteogenesis. *Biomaterials* **2005**, *26*, 5474–5491. [CrossRef] [PubMed]
40. Salerno, A.; Guarnieri, D.; Iannone, M.; Zeppetelli, S.; di Maio, E.; Iannace, S.; Netti, P.A. Engineered μ-Bimodal Poly(ε-Caprolactone) Porous Scaffold for Enhanced HMSC Colonization and Proliferation. *Acta Biomater.* **2009**, *5*, 1082–1093. [CrossRef] [PubMed]
41. Silva, M.M.C.G.; Cyster, L.A.; Barry, J.J.A.; Yang, X.B.; Oreffo, R.O.C.; Grant, D.M.; Scotchford, C.A.; Howdle, S.M.; Shakesheff, K.M.; Rose, F.R.A.J. The Effect of Anisotropic Architecture on Cell and Tissue Infiltration into Tissue Engineering Scaffolds. *Biomaterials* **2006**, *27*, 5909–5917. [CrossRef]
42. Salerno, A.; Zeppetelli, S.; di Maio, E.; Iannace, S.; Netti, P.A. Design of Bimodal PCL and PCL-HA Nanocomposite Scaffolds by Two Step Depressurization During Solid-State Supercritical CO $_2$ Foaming. *Macromol. Rapid Commun.* **2011**, *32*, 1150–1156. [CrossRef]
43. García-Casas, I.; Montes, A.; Valor, D.; Pereyra, C.; de la Ossa, E.J.M. Foaming of Polycaprolactone and Its Impregnation with Quercetin Using Supercritical CO_2. *Polymers* **2019**, *11*, 1390. [CrossRef]
44. Campardelli, R.; Franco, P.; Reverchon, E.; de Marco, I. Polycaprolactone/Nimesulide Patches Obtained by a One-Step Supercritical Foaming + Impregnation Process. *J. Supercrit. Fluids* **2019**, *146*, 47–54. [CrossRef]
45. Yoganathan, R.; Mammucari, R.; Foster, N.R. Impregnation of Ibuprofen into Polycaprolactone Using Supercritical Carbon Dioxide. *J. Phys. Conf. Ser.* **2010**, *215*, 12087. [CrossRef]
46. Godoy-Gallardo, M.; Portolés-Gil, N.; López-Periago, A.M.; Domingo, C.; Hosta-Rigau, L. Multi-Layered Polydopamine Coatings for the Immobilization of Growth Factors onto Highly-Interconnected and Bimodal PCL/HA-Based Scaffolds. *Mater. Sci. Eng. C* **2020**, *117*, 111245. [CrossRef] [PubMed]
47. Khodaverdi, E.; Reza Abbaspour, M.; Oroojalian, F.; Omidkhah, N.; Hossein-nezahd, S.; Kamali, H.; Hadizadeh, F. Dexamethasone Delivery of Porous PEG-PCL-PEG Scaffolds with Supercritical Carbon Dioxide Gas Foaming. *J. Drug Deliv. Sci. Technol.* **2021**, *66*, 102547. [CrossRef]
48. Collins, N.J.; Leeke, G.A.; Bridson, R.H.; Hassan, F.; Grover, L.M. The Influence of Silica on Pore Diameter and Distribution in PLA Scaffolds Produced Using Supercritical CO_2. *J. Mater. Sci. Mater. Med.* **2008**, *19*, 1497–1502. [CrossRef]
49. Salerno, A.; Iannace, S.; Netti, P.A. Open-Pore Biodegradable Foams Prepared via Gas Foaming and Microparticulate Templating. *Macromol. Biosci.* **2008**, *8*, 655–664. [CrossRef]
50. Kim, J.-W.; Shin, K.-H.; Koh, Y.-H.; Hah, M.J.; Moon, J.; Kim, H.-E. Production of Poly(ε-Caprolactone)/Hydroxyapatite Composite Scaffolds with a Tailored Macro/Micro-Porous Structure, High Mechanical Properties, and Excellent Bioactivity. *Materials* **2017**, *10*, 1123. [CrossRef]
51. Markočič, E.; Škerget, M.; Knez, Ž. Solubility and Diffusivity of CO_2 in Poly(l-Lactide)–Hydroxyapatite and Poly(d,l-Lactide-Co-Glycolide)–Hydroxyapatite Composite Biomaterials. *J. Supercrit. Fluids* **2011**, *55*, 1046–1051. [CrossRef]
52. Adamović, T.; Milovanović, S.; Marković, D.; Žižović, I. Impregnation of Cellulose Acetate Films with Carvacrol Using Supercritical Carbon Ioxide. *Tehnika* **2018**, *73*, 19–25. [CrossRef]
53. Nowak, M.; Misic, D.; Trusek, A.; Zizovic, I. Polymeric Microfiltration Membranes Modification by Supercritical Solvent Impregnation—Potential Application in Open Surgical Wound Ventilation. *Molecules* **2021**, *26*, 4572. [CrossRef]
54. Lukic, I.; Vulic, J.; Ivanovic, J. Antioxidant Activity of PLA/PCL Films Loaded with Thymol and/or Carvacrol Using $ScCO_2$ for Active Food Packaging. *Food Packag. Shelf Life* **2020**, *26*, 100578. [CrossRef]
55. Benkaddour, A.; Jradi, K.; Robert, S.; Daneault, C. Grafting of Polycaprolactone on Oxidized Nanocelluloses by Click Chemistry. *Nanomaterials* **2013**, *3*, 141–157. [CrossRef] [PubMed]
56. Valderrama, A.C.S.; Rojas De, G.C. Traceability of Active Compounds of Essential Oils in Antimicrobial Food Packaging Using a Chemometric Method by ATR-FTIR. *Am. J. Anal. Chem.* **2017**, *08*, 726–741. [CrossRef]
57. Gheisari, H.; Karamian, E.; Abdellahi, M. A Novel Hydroxyapatite—Hardystonite Nanocomposite Ceramic. *Ceram. Int.* **2015**, *41*, 5967–5975. [CrossRef]
58. Leeke, G.; Santos, R.B.; King, M. Vapor−Liquid Equilibria for the Carbon Dioxide + Carvacrol System at Elevated Pressures. *J. Chem. Amp. Eng. Data* **2001**, *46*, 541–545. [CrossRef]